ARTICLE IN PRESS

PERGAMON

Aerosol Science ▮▮▮ (▮▮▮▮) ▮▮▮–▮▮▮

Journal of
Aerosol Science

www.elsevier.com/locate/jaerosci

Refractive index of aerosol particles over the Amazon tropical forest during LBA-EUSTACH 1999

Pascal Guyon[a,*], Olivier Boucher[b,c], Bim Graham[a], Jens Beck[a], Olga L. Mayol-Bracero[a], Gregory C. Roberts[a], Willy Maenhaut[d], Paulo Artaxo[e], Meinrat O. Andreae[a]

[a] *Department of Biogeochemistry, Max Planck Institute for Chemistry, POB 3060 Biogeochemistry, 55020 Mainz, Germany*
[b] *Department of Atmospheric Chemistry, Max Planck Institute for Chemistry, Mainz, Germany*
[c] *Laboratoire d'Optique Atmosphérique, CNRS/USTL, Villeneuve d'Ascq, France*
[d] *Institute for Nuclear Sciences, Ghent University, Gent, Belgium*
[e] *Institute for Physics, University of São Paulo, São Paulo, Brazil*

Received 4 July 2002; accepted 1 March 2003

Abstract

Optical properties of aerosol particles were characterized during two field campaigns at a remote rainforest site in Rondônia, Brazil, as part of the project European Studies on Trace Gases and Atmospheric Chemistry, a contribution to the Large-Scale Biosphere-Atmosphere Experiment in Amazonia (LBA-EUSTACH). The measurements included background (wet season), biomass burning (dry season), and transition period conditions. Optical measurements of light scattering and absorption were combined with data on number/size distributions in a new iterative method, which retrieves the effective imaginary refractive index of the particles at a wavelength of 545 nm. For ambient relative humidities lower than 80%, background aerosols exhibited an average refractive index of $1.42 - 0.006i$. Biomass burning aerosols displayed a much larger imaginary part, with an average refractive index of $1.41 - 0.013i$. Other climate-relevant parameters were estimated from Mie calculations. These include single-scattering albedos of 0.93 ± 0.03 and 0.90 ± 0.03 (at ambient humidity), asymmetry parameters of 0.63 ± 0.02 and 0.70 ± 0.03, and backscatter ratios of 0.12 ± 0.01 and 0.08 ± 0.01 for background and biomass burning aerosols, respectively.

Keywords: Aerosol optical properties; Scattering coefficient; Absorption coefficient; Size distribution; Optical particle counter; Biomass burning

* Corresponding author. Tel.: +49-6131-305404; fax: +49-6131-305487.
E-mail addresses: guyon@mpch-mainz.mpg.de (P. Guyon), boucher@loa.univ-lille1.fr (O. Boucher), bim.graham@csiro.au (B. Graham), jbeck@gwdg.de (J. Beck), omayol@sunites.upr.clu.edu (O.L. Mayol-Bracero), greg@fiji.ucsd.edu (G.C. Roberts), Willy.Mainhaut@rug.ac.bc (W. Maenhaut), artaxo@if.usp.br (P. Artaxo), moa@mpch-mainz.mpg.de (M.O. Andreae).

0021-8502/03/$ - see front matter © 2003 Published by Elsevier Science Ltd.
doi:10.1016/S0021-8502(03)00052-1

1. Introduction

Optical particle counters (OPCs) are frequently used to determine the size distribution of aerosol particle populations (see, for example, Reid et al., 1998a; Collins et al., 2000; Redemann et al., 2000). OPCs measure the magnitude of light scattering by individual aerosol particles and then use an internal calibration function to determine their size. The scattering coefficients of a population of aerosols can then be retrieved from the size distribution by performing Mie calculations. Comparisons of scattering coefficients calculated in this way with those measured directly using an integrating nephelometer have been reported previously (see, for example, Stolzenburg, Kreisberg, & Hering, 1998; Collins et al., 2000; Liu & Daum, 2000).

OPCs are usually calibrated using latex particles, which have a refractive index of $m = 1.588 - 0i$. These particles are highly efficient at scattering radiation, as indicated by the large real component of the refractive index, and are completely non-absorbing (no imaginary component). Ambient particles, by comparison, are usually less efficient scatterers of radiation, but display some absorptive properties. Consequently, OPCs generally underestimate the true diameter of ambient aerosols, and the measured size distributions should be corrected for the refractive index of the sampled particles. In most instances, however, this is not a trivial task because it is very difficult to determine the refractive index of ambient aerosol particles that have complex chemical compositions; indeed, the refractive index remains one of the least well-characterized properties of such aerosols.

Aerosol models tend to predict more and more of the details of the aerosol microphysics (size distribution, chemical composition, and state of mixture), from which the aerosol optical properties need to be computed. Such a modeling approach requires new techniques to estimate an aerosol refractive index from observations, which can serve as a test for the models. Because it is not feasible to determine the refractive index of each individual particle within an aerosol population, an "average" or effective refractive index is normally used to represent the whole size distribution. This parameter is most often derived from the volume average of the chemical composition of the aerosols (e.g., Horvath, 1998). Such an approach makes the assumption that the particles are uniformly internally mixed and, ideally, requires a complete knowledge of the aerosol particle composition (mass closure) (e.g., Pesava, Horvath, & Kasahara, 2001; Ebert et al., 2002), as well as the refractive indices and densities of all the individual compounds (or classes of compounds) present in the aerosol particles. In practice, however, typically only the two or three compound classes that contribute most significantly to the scattering and absorption of light by the aerosols are considered.

An alternative approach to determining the appropriate index of refraction to derive corrected size distributions from the raw OPC data is to use an iterative process. On the simplest level, this involves varying the index of refraction until the scattering coefficients that one derives from the corresponding OPC size distributions (using Mie calculations) agree most closely with those measured directly with, for example, an integrating nephelometer. Liu and Daum (2000) estimated that an error of nearly 60% in the estimation of the total scattering coefficient would result from not correcting the OPC (in their case a passive cavity aerosol spectrometer probe, PCASP) size distribution for the particle refractive index prior to calculating the light scattering coefficients. Usually, the contribution of absorption to the extinction of radiation by the aerosols has been ignored in such iterative calculations. This, however, may be an additional important factor to consider, because an absorbing aerosol will

scatter light less effectively than an otherwise identical, non-absorbing aerosol. The real (scattering) component of the refractive index obtained by only considering the scattering of radiation by aerosols will therefore be overestimated, and the diameters will be underestimated.

In this article we present a new, more comprehensive approach to the correction of size distribution data measured by OPCs and the retrieval of effective refractive indices for aerosol populations. Additionally, we derive values of the asymmetry parameter (g), the single-scattering albedo (ω_0), and the backscattered fraction (β) ratio using further Mie calculations. The approach is similar to the iterative one described above, but takes into account both the scattering and absorption properties of aerosols, as determined through in situ measurements of the same air mass sampled by an OPC. In our case, we use size distribution data collected with a PCASP, in combination with scattering and absorption coefficients measured using an integrating nephelometer and a particle soot absorbance photometer (PSAP), respectively.

The overall method is demonstrated using data collected over an undisturbed primary tropical forest in Rondônia, Brazil, during the LBA-EUSTACH campaigns (Andreae et al., 2002). The development of accurate methods for measuring aerosol parameters of climatic relevance is particularly pertinent to the study of aerosols in regions such as this for a variety of reasons (Boucher & Haywood, 2001). First, Brazil contains the world's largest rainforest, which provides a constant release of biogenic aerosols, formed either by direct emission (primary) or through gas-to-particle conversion of gases emitted by vegetation (secondary). In addition, each year a massive injection of smoke aerosols occurs during the dry season due to widespread biomass burning. The intense convective activity associated with the tropics means that these aerosols may be rapidly uplifted to high altitudes, where they can be transported over long distances and have effects on regional and global climate (Pickering et al., 1996; Andreae et al., 2001; Staudt et al., 2001).

2. Instrumentation and methods

2.1. Sampling conditions

Measurements were made near the top of a 54-m high measurement tower during two field campaigns that took place in April–May 1999 (LBA-EUSTACH 1) and September–October 1999 (LBA-EUSTACH 2). The tower was located at 10°04′55″ S, 61°55′48″ W, 110 m above sea level, in the Jarú Biological Reserve—a primary tropical forest situated in the Brazilian state of Rondônia. LBA-EUSTACH 1 encompassed the end of the wet season and the transition toward the biomass-burning-influenced dry season. LBA-EUSTACH 2 was largely dominated by biomass burning conditions. All instruments were placed 52–54 m above ground level (ca. 22 m above maximum canopy height), except where indicated otherwise, to ensure sampling of a regionally representative air mass. The sampling site is described in detail in Andreae et al. (2002).

2.2. Instrumentation

2.2.1. Size distributions

Size distributions were measured with a laser optical instrument—the PCASP-100x (DMT, USA, now owned by Particle Metrics, Longmont, USA). The PCASP is an OPC that measures the size

distribution of aerosol particles of nominal diameters from 0.1 to 3 μm in 18 channels. The instrument derives the size of particles from the degree to which they individually scatter light at a wavelength of 633 nm between scattering angles of 35–135°. The instrument is calibrated by the manufacturer using spherical polystyrene latex particles of known diameter and with a refractive index of 1.588 − 0i, so that the size distribution output from the PCASP should be considered as "latex equivalent."

Successful operation of the PCASP requires that the particles pass through the radiation beam in the internal chamber of the instrument one at a time, so that the scattering efficiency can be measured for each individual particle. High particle concentrations ($> 10\,000\ \mathrm{cm}^{-3}$) may lead to particle coincidence, and therefore counting and sizing errors (Reid, 1998). Such conditions were only encountered occasionally and the data collected during these periods was excluded from further analysis. Reid (1998) also estimated the uncertainty in particle number concentration measured from the PCASP to be less than 10%. Because the error in particle number concentration can, for the most part, be attributed to the particle coincidence effect, we considered the PCASP to measure the concentration with a 10% accuracy at high particle concentration (Reid, 1998), as encountered during the LBA-EUSTACH 2 campaign, and with a 5% accuracy during the wet season campaign, when particle number concentration was about one order of magnitude lower.

In order not to significantly alter the properties of the sampled ambient aerosols, the de-icing heater that is situated at the inlet of the PCASP instrument was not used, and the sheath flow was not dried with silica gel. Collins et al. (2000) estimated the total internal temperature increase of the instrument to be about 3.5 ± 2°C, which reduces the relative humidity (RH) inside the instrument by about 10–15%, under the conditions of RH and temperature encountered.

The mass/size distribution of the aerosols was also measured with a microorifice uniform deposit impactor (MOUDI, model 110, MSP corporation, Minneapolis, USA). Aerosols of aerodynamic diameter between 18 and 0.051 μm were collected in 10 fractions with calibrated D_{50} aerodynamic cutoffs of 18, 9.9, 6.2, 3.1, 1.8, 1.0, 0.578, 0.346, 0.200, 0.093, and 0.051 μm. Mass concentrations were obtained by weighing, after having been left equilibrating under controlled conditions of RH (50%) and temperature (20°C) for at least 24 h. The accuracy of the measurements is of the order of ±3 μg for aluminum foils and ±5 μg for Nuclepore filters.

2.2.2. Scattering coefficients

Scattering coefficients were measured using a single-wavelength integrating nephelometer (model M903, Radiance Research, Seattle, USA) at a wavelength of 545 nm. Aerosols were sampled continuously and were partially dried out by the heat produced by the instrument itself. The RH was measured inside the instrument and was found to be on average 15% (±6%) lower than ambient, comparable to that inside the PCASP. The instrument measures light scattering between the angles of 8.9° and 170°. In this study, the error associated with truncation of the very forward and very backward scattering angles was parameterized in our Mie calculations, and the error in the scattering coefficients was estimated to be only the random measurement error associated with the instrument itself (of the order of 5%).

2.2.3. Absorption coefficients

Continuous absorption measurements at a center wavelength of 565 nm were made using a particle soot absorption photometer (PSAP, Radiance Research, Seattle, USA). Absorption coefficients, σ_a,

were retrieved according to Reid et al. (1998b) and Bond, Anderson, and Campbell (1999), and associated uncertainties calculated according to Bond et al. (1999) and Anderson et al. (1999). In our case, the 95% confidence interval for instrument noise, obtained from filtered air measurements, was found to be 0.008 Mm^{-1} for hourly time resolution, much smaller than the value of 0.11 Mm^{-1} obtained by Anderson et al. (1999) for the same time resolution.

2.2.4. Aerosol composition

To characterize the chemical composition of the aerosols, the concentrations of organic carbon (OC), apparent elemental carbon (EC_a), black carbon, eight ions (Na^+, NH_4^+, K^+, Mg^{2+}, Ca^{2+}, NO_3^-, SO_4^{2-}, Cl^-), and up to 17 elements (Al, Si, P, S, Cl, K, Ca, Ti, Cr, Mn, Fe, Cu, Zn, Br, Sr, Zr, and Pb) in the aerosols were measured on filter samples.

Elemental composition and total mass concentrations were obtained via analysis of samples collected on Nuclepore filters using a stacked filter unit (SFU), with two filters in series being used to collect the particles in the coarse ($2.0 < D < 10$ μm) and fine ($D < 2.0$ μm) mode. Elemental concentrations were obtained by particle-induced X-ray emission analysis (PIXE), mass concentrations by weighing. Black carbon equivalent (BC_e) concentrations were obtained for the fine fraction of the SFU filters by a light reflectance technique (Andreae, 1983). For more details concerning the SFU filters sampling and analysis, see Artaxo et al. (2002).

OC and EC_a analyses were performed on quartz-filter aerosol samples using a thermal optical transmission (TOT) technique (Birch & Cary, 1996). Elemental carbon is usually assumed to be the only light absorbing matter in aerosols (with the exception of metal oxides, normally present in negligible quantities). The TOT technique corrects for the artifact EC formed by charring during pyrolysis of the organic compounds by defining as EC_a only the carbon that evolves after the light transmittance through the sample has reached the original transmittance. Nevertheless, uncertainties in the discrimination between EC_a and OC may arise from the fact that some organic compounds may also be light absorbing. Furthermore, it has been found that the relative amounts of OC and EC_a, as provided by the TOT technique, can depend on the temperature program used for certain sample types (Yu, Xu, & Yang, 2002; Maenhaut, unpublished results) and that the technique may provide too low EC_a/OC for heavily loaded filter samples (Kubátová, Vermeylen, Claeys, Cafmeyer, & Maenhaut, 1999). The samples were collected with a high-volume dichotomous sampler (HVDS) (Solomon, Moyers, & Fletcher, 1983), which splits the aerosol into two size fractions (particles of D smaller and larger than ca. 2.5 μm). A detailed description of the filter collection and handling procedure is provided in Mayol-Bracero et al. (2002).

The concentrations of selected ions in the quartz filter samples were determined by standard ion chromatographic techniques, incorporating background ion suppression and conductivity detection (Elbert, Hoffmann, Kramer, Schmitt, Andreae, 2000).

2.3. Correction of PCASP-derived size distributions and calculation of refractive indices

2.3.1. Description of the model

The method we propose for calculating the refractive index of atmospheric particles, and for correcting the size distribution data from the PCASP is based on an iterative process, outlined schematically in Fig. 1. A modified size distribution is calculated from the initial size distribution retrieved from the PCASP, using a variable refractive index, $m_{assumed}$. The program used to calculate

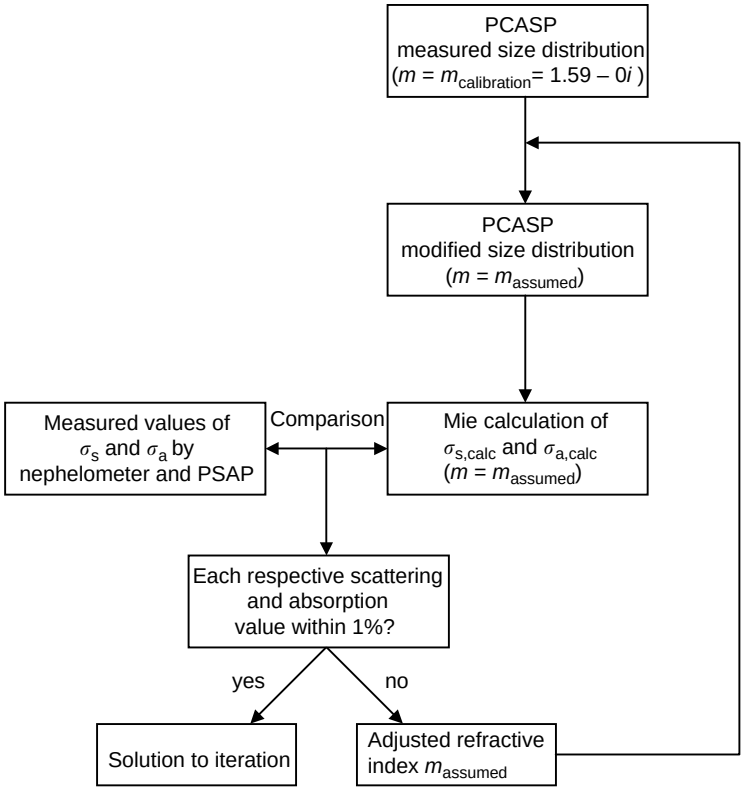

Fig. 1. Flow chart of the iteration method used for retrieving the effective refractive index and corrected size distribution of atmospheric aerosols using size distribution (PCASP), absorption (PSAP), and nephelometer scattering data.

the new size distribution is essentially the one distributed by the manufacturer, but modified to allow for a wider range and precision of refractive indices. Scattering and absorption coefficients are obtained by performing Mie calculations on the modified size distribution, using the same assumed refractive index, $m_{assumed}$, at a wavelength of 545 nm (the wavelength at which the nephelometer operates, and close to that used by the PSAP (565 nm)). The calculated scattering and absorption coefficients ($\sigma_{s,calc}$ and $\sigma_{a,calc}$, respectively) are then compared to the measured values (σ_s and σ_a, respectively), and the refractive index, $m_{assumed}$, adjusted until both $\sigma_{s,calc}$ and $\sigma_{a,calc}$ are within 1% of σ_s and σ_a, respectively (2% for the LBA-EUSTACH 1 data set because of the low measured σ_s and σ_a).

PCASP, PSAP, and nephelometer data were averaged hourly for both measurement campaigns, and the model applied to all data points for which data of the three instruments were available. Initially, the real component of the refractive index was allowed to vary between 1.33 (that of water) and 1.59 (that of latex) in incremental steps of 0.01, whilst the imaginary part could range from 0 to $0.05i$, with 0.005 incremental steps. Incremental steps were then set to 0.005 and 0.0025 for the real and the imaginary refractive index values, respectively, when $\sigma_{s,calc}$ and $\sigma_{a,calc}$ approached within 5% of the measured σ_s and σ_a values.

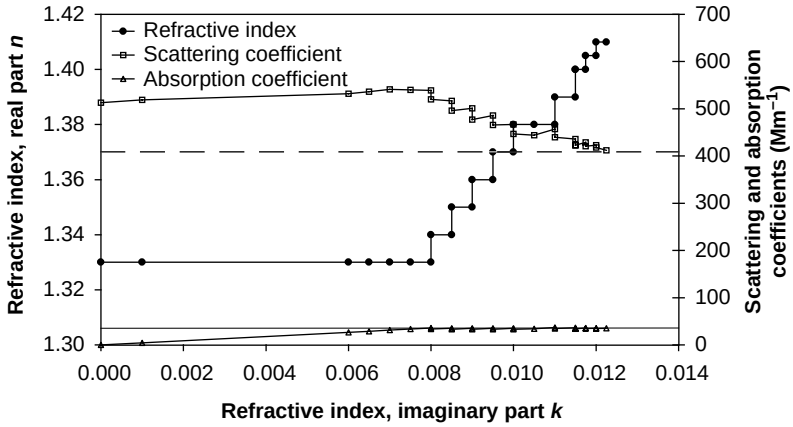

Fig. 2. Example of the iterative calculation procedure for a typical data set from the LBA-EUSTACH 2 campaign (6 October 1999, 1400 local time). The graph shows the convergence of the calculated scattering (open squares) and absorption (open triangles) coefficients towards the measured scattering (dashed line) and absorption (horizontal line) coefficients, together with the calculated complex refractive index, $m = n - ik$ (black dots).

An example of a convergent solution obtained with our iteration procedure is given in Fig. 2, for a representative data set from the LBA-EUSTACH 2 campaign (similar convergent behavior was observed for data sets from the first campaign, except that a solution was generally found in fewer steps due to the typically lower refractive index observed during the wet season). The iteration was initiated with both parts of the refractive index, m_{assumed}, set to the minimum values (i.e., the real part $n = 1.33$ and the imaginary part $k = 0$). The imaginary part was then increased until $\sigma_{\text{a,calc}}$ matched σ_{a} within $\pm 5\%$. An increasing imaginary part has the effect of increasing the corrected particle sizes, resulting in an increase in the corresponding $\sigma_{\text{s,calc}}$ value, along with $\sigma_{\text{a,calc}}$. When $\sigma_{\text{a,calc}}$ reached σ_{a} (at $m = 1.33 - 0.008i$ in this example), the calculated scattering coefficient, $\sigma_{\text{s,calc}}$, was always found to be greater than the observed one (represented by the dashed line), and the size of the particles was overestimated (due to the low real and high imaginary components of the refractive index). The real part of m_{assumed} was subsequently increased, decreasing the corrected sizes of the particles, together with the values of $\sigma_{\text{s,calc}}$ and $\sigma_{\text{a,calc}}$. The value of the imaginary part had to be readjusted once more and $\sigma_{\text{a,calc}}$ was found to start to oscillate around the observed value (the dotted line), while $\sigma_{\text{s,calc}}$ converged towards its solution.

The iterative calculations always converged toward a unique solution within the range of refractive indices open to the model, except in some unusual cases. These were all characterized by a high ambient RH, close to 100% or at least greater than 92%, which mostly occurred at night or in the early morning hours. Under these conditions, the inability to reconcile the data from the three online instruments using the iteration procedure is probably due to the erratic responses of the nephelometer and PCASP at high RH, resulting from the steep growth function of the particles in this RH range. In light of this fact, only measurements made at ambient RH below 80% were considered in our subsequent analyses. Figs. 3a and b show the refractive indices calculated by the iteration procedure for all such data sets, for the LBA-EUSTACH 1 and 2 campaigns, respectively. The behavior of the refractive index with increasing RH will be discussed below.

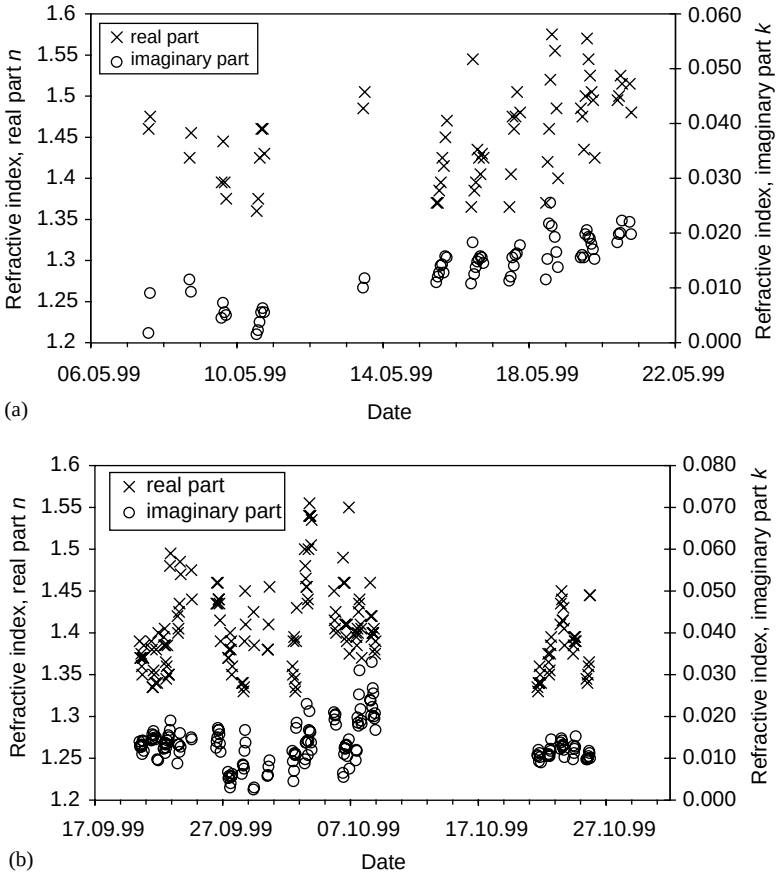

Fig. 3. (a) Refractive indices calculated using the iteration procedure for the LBA-EUSTACH 1 campaign. Only data measured at an RH $< 80\%$ are presented. (b) Refractive indices calculated using the iteration procedure for the LBA-EUSTACH 2 campaign. Only data measured at an RH $< 80\%$ are presented.

2.3.2. *Applicability of the model*

A critical assumption made in our Mie calculations is that the aerosols are spherical in shape and homogeneously internally mixed. This assumption is most critical for aerosol particles in the accumulation mode (i.e., particles with diameters ranging from ca. 0.1–1 μm), since these are known to be the most efficient at scattering and absorbing light. Particles in the accumulation mode usually arise from the coagulation of smaller particles or from the condensation of low volatility vapors. They are also involved in cloud processing and are subject to water uptake and growth at high RH, forming spherical wet aerosols or solution droplets.

Although the water content of the aerosols was not measured during LBA-EUSTACH 1 and 2, it is probable that most of the sampled aerosols had been through at least one cycle of cloud or fog formation. In the Amazon, each volume of air cycles through a convective cloud about twice a day (Miller et al., 1985), and an air parcel is likely to be processed through 10 or more non-precipitating cloud cycles (Hoppel, Fitzgerald, Frick, Larson, & Mack, 1990). Fog was often observed in the mornings during both seasons. Moreover, it is likely that the aerosols still

had a significant water content upon collection, due to the consistently high humidity encountered during both seasons. During LBA-EUSTACH 1, the ambient relative humidity (RH) was greater than 64% for 95% of the time, and in the range 98–100% for 50% of the time. For LBA-EUSTACH 2, the RH was greater than 48% for 95% of the time, and 98–100% for 31% of the time.

All of the above observations lead us to the conclusion that the majority of particles in the accumulation mode had most likely deliquesced prior to sampling and still contained some water when sampled during the LBA-EUSTACH campaigns. Therefore, our treatment of the accumulation mode as spherical, internally mixed particles in the Mie calculations is a reasonable approximation.

Particles in the Aitken mode (i.e., particles below ca. 0.1 μm in diameter), and particles in the mechanically generated coarse mode (diameter larger than ca. 1 μm) are more likely to be non-spherical. Particles in the Aitken mode do not usually contribute significantly to the optical properties of an aerosol population. Moreover, particles that are much smaller in size than the wavelength considered (545 nm) have a phase function comparable to those of spheres anyway. The presence of a large amount of coarse mode aerosol with non-spherical geometries may lead to some errors in the Mie approximation. To assess this potential source of error in our case, we calculated mass scattering efficiencies (α_s) and mass absorption efficiencies (α_a) for both the coarse (10 μm $> D >$ 2 μm) and fine ($D <$ 2 μm) mode aerosol fractions by multivariate regression, using the data obtained with the nephelometer, PSAP, and SFU filters (Guyon et al., 2003). The results indicate that coarse mode particles did not contribute significantly to the scattering during either field campaign. The value of α_a for the coarse fraction was found to be significant during LBA-EUSTACH 2, but the fine particle mass was dominant during this campaign. During LBA-EUSTACH 1, α_a for the coarse fraction was approximately a third that of the fine fraction, corresponding to a contribution by the coarse mode of 30–60% to the total absorption. In the latter case, the scattering and absorption by the coarse mode particles correlated well with mineral dust elements (i.e., Al, Fe, Mn, and Si), a finding that is particularly noteworthy in light of the modeling studies of Mishchenko, Travis, Kahn, and West (1997). They found that although aerosol shape may have dramatic effects on the scattering phase function (especially for the side and back scattering angles), other optical characteristics (the extinction, scattering and absorption cross sections, single-scattering albedo, asymmetry parameter, and the backscatter fraction) of spherical particles differ by only a few percent from those of modeled particles representative of mineral dust, with the difference decreasing with increasing particle size. Therefore, treating the coarse mode aerosol as spherical in nature is likely to have led to only small overall errors in our analyses.

Focusing on aerosols derived from biomass burning, Martins, Hobbs, Weiss, and Artaxo (1998) measured the degree of non-sphericity (α_0) of particles in Brazil during the Smoke, Clouds, and Radiation-Brazil (SCAR-B) experiment, using electro-optical light-scattering measurements and scanning electron microscopy. They concluded that smoke particles more than 1-h old have a value of α_0 lower than 13% in all cases, and lower than 4% in 72% of cases, indicating that smoke particles are, for the most part, close to spherical in shape, in agreement with other previous measurements (Hallett, Hudson, & Rogers, 1989; Westphal & Toon, 1991). Thus, for these particles there is additional strong experimental evidence that Mie calculations can be applied without the introduction of significant errors.

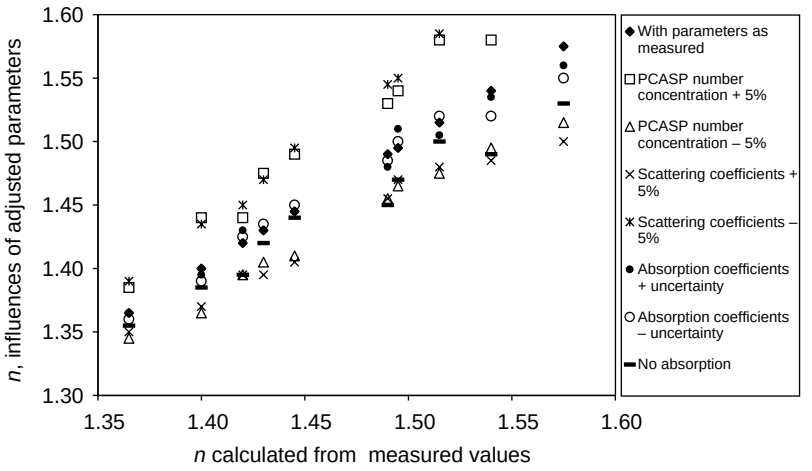

Fig. 4. Sensitivity of the real part of the refractive index to changes in the individual parameters used in the iteration calculations for the LBA-EUSTACH 1 campaign. This sensitivity test was applied to ten representative data sets from the LBA-EUSTACH 1 campaign.

An additional potential source of error in our analyses arises from the fact that the size distribution measured by the PCASP instrument has a lower cutoff diameter at 0.1 μm, so that the tail of the accumulation mode and the whole Aitken mode are not measured, whereas the nephelometer and the PSAP measure the aerosol properties integrated over the whole aerosol population. However, as discussed previously, the contribution of the Aitken mode to the overall optical properties of the aerosols relative to the accumulation mode is negligible. Liu and Daum (2000) estimated the magnitude of this effect and concluded that, in their case, the relative contribution of particles with diameters of 0.05–0.1 μm to the total light-scattering coefficient calculated from the truncated size distribution (with the lower cutoff diameter at 0.1 μm) was of the order of only ca. 2%. We had no reason to suspect that the contribution of particles smaller than 0.1 μm to scattering and absorption might be more significant in our case, and so we restricted ourselves solely to consideration of the size distribution as measured by the PCASP instrument.

2.3.3. *Sensitivity of the model*

In order to estimate the accuracy of the values of the refractive index calculated from the iteration procedure, we individually varied different parameters used in the iteration by an amount equal to the error estimates for the nephelometer, PSAP, and PCASP instruments (given in the previous sections of this article), whilst the other parameters were kept equal to their original values. These sensitivity tests were applied to ten cases representative of both field campaigns. As an example, Fig. 4 shows the sensitivity of the real part of the refractive index to changes in the individual parameters for the LBA-EUSTACH 1. Overall, the precision was typically better than 5% for n and 10% for k for the largest values of n and k within the range of observed refractive indices (the precision decreases with increasing n and k values). This indicates that, given the accuracies of our measurements, this new procedure is quite a robust method for estimating refractive indices.

3. Results and discussion

3.1. Effective refractive indices derived from the iteration procedure

The refractive indices calculated for LBA-EUSTACH 1 and 2 using the iteration procedure, for ambient RH lower than 80%, are shown in Figs. 3a and b, respectively. In the first instance, a single effective refractive index was calculated to represent the whole size distribution measured by the PCASP. Despite the fact that the coarse mode particles (diameter greater than ca. 1 μm) are usually expected to have a refractive index with a lower imaginary part than that of the fine mode particles, this approach is justified by the fact that particles of both modes showed similar absorption properties (Section 2.3.2), leading to little influence on the effective refractive index of the aerosol population. This assumption is discussed later in more detail for both wet and dry season data.

A noticeable feature of the LBA-EUSTACH 1 data is the large increase in the imaginary part, and to a lesser extent in the real part, of the refractive index upon entering the transition period toward the burning season. Values of the refractive index for the first part of the LBA-EUSTACH 1 campaign (7–12 May 1999) are centered on $m = 1.42(\pm 0.04) - 0.006(\pm 0.003)i$, reaching $1.46(\pm 0.06) - 0.016(\pm 0.006)i$ at the end of the campaign (13–21 May 1999), a value comparable to that obtained for the biomass burning period (LBA-EUSTACH 2). The observed increase for the imaginary part of the refractive index can be attributed to an increase in the black carbon content of the aerosol, associated with a general buildup in fire activity in Brazil. This increase in fire activity toward the end of the LBA-EUSTACH 1 campaign is clearly evident from fire pixel data measured by the NOAA-12 satellite (available from CPTEC at http://www.cptec.inpe.br/products/queimadas/).

It is worthnoting that there were no fire pixels detected in the state of Rondônia, where the measurements took place during LBA-EUSTACH 1. However, back trajectories calculated for this period showed air masses coming from the neighboring states of Mato Grosso, Mato Grosso do Sul, and Goias, which contributed to most of the fire activity in the region. These biomass-burning-influenced air masses required some 2–3 days to reach the sampling site, providing sufficient time for the aerosols to be subjected to cloud processing, and thus justifying the treatment of the aerosols as internally mixed particles in our model calculations for this period (Horvath, 1998). On the basis of these observations, we consider the refractive index calculated for the first part of LBA-EUSTACH 1 as representative of background Amazonian aerosol, and that found for the end of this campaign as typical of aged biomass-burning aerosol.

A daily variation in refractive index was observed that is most likely attributable to changes in ambient RH, although no significant correlation could be established, probably because of the variability of the aerosol sources and composition with time. Overall, the refractive index decreased with increasing RH. At high ambient RH, the real part of the refractive index approached that of water (1.33); however, the imaginary part showed less variation, usually not reaching zero.

The refractive indices obtained for the second campaign (Fig. 3b) showed a larger variability (as did the other aerosol measurements), partly attributable to the variation in RH, but mainly because of the passage of smoke plumes from nearby fires. The refractive indices found for this campaign are most representative of aerosols belonging to haze and younger smoke plumes.

3.2. Comparison with refractive indices estimated from the volume-averaged chemical composition

We compared the refractive indices obtained from the iteration model with volume-average estimates calculated from the chemical composition of the aerosols (e.g., Horvath, 1998) for three periods of interest: (1) LBA-EUSTACH 1, before the transition period (representative of background, wet season conditions), (2) LBA-EUSTACH 1, during the transition period toward the biomass-burning-influenced, dry season period, and (3) LBA-EUSTACH 2, largely dominated by biomass burning conditions. We limited ourselves to volume-average calculations involving four classes of compounds only: black carbon (either BC_e or EC_a), hematite (Fe_2O_3, present in non-negligible amounts, especially during LBA-EUSTACH 1), particulate organic matter (POM), and inorganic non-absorbing matter (INAM). INAM was calculated as the sum of all inorganic species (except for hematite), assuming the PIXE-detected inorganic elements to be present in the aerosol in the state of their most common oxide (Mason & Moore, 1982). POM (fine fraction only) was estimated by subtracting the sum of oxides, ions, and elemental carbon from the total mass of aerosol in the fine fraction filter samples.

Calculations of the volume average of the refractive index were performed using the density and refractive index of each class of compound as prescribed by Horvath (1998) (except when indicated otherwise). According to the literature, the refractive index of soot, at wavelengths close to 550 nm, can vary from 1.3 to 2.5 for the real part and from 0.1 to 1 for the imaginary part (Fuller, Malm, & Kreidenweis, 1999; Marley et al., 2001). Its density ranges from 625 to 2250 kg m^{-3}, depending on the type of soot considered (Fuller et al., 1999). We chose the commonly accepted refractive index value o $1.50-0.47i$, and a density of 1200 kg m^{-3}. The refractive indices and specific densities of POM and INAM are also subject to much uncertainty. We used values of $1.40-0i$ and 1200 kg m^{-3} for POM (Turpin & Lim, 2001), and $1.50-0i$ and 1800 kg m^{-3} for INAM. For hematite, we used a refractive index of $3.0-0.60i$ and a density of 4500 kg m^{-3} (Sokolik & Toon, 1999).

Tables 1a and b summarize the volume average of POM, inorganic matter, hematite, and black carbon from the mass closure described above, as well as the corresponding calculated range of refractive indices, separated into real (n) and imaginary (k) parts, for the three periods described above. The refractive indices were calculated using the sulfate concentrations derived from the PIXE S measurements rather than the IC analysis of the quartz filters because the latter are known to adsorb SO_2 and H_2SO_4 (Savoie, Prospero, & Nees, 1987) from the gas phase. The calculations were performed using either the EC_a content measured on the quartz filters (Table 1a) or BC_e determined from the Nuclepore filters (Table 1b). BC_e already takes into account the contribution of hematite to absorption, and this compound was therefore not included in the calculations of Table 1b. The last two columns of each table show the averaged real and imaginary parts as obtained from the iteration procedure for each period.

Considering first the real parts of the refractive indices, the values obtained from the iteration model are in the range of the volume-average estimates. It should be noted, however, that the latter values do not take into account the water content of the aerosols, whereas values from the iteration procedure were derived from ambient condition measurements (as discussed in Section 2.3). Accounting for water (with a refractive index m_{water} of $1.33-0i$) in the volume-average calculations is expected to lower these calculated values.

The values of the imaginary part of the refractive indices obtained by the iteration procedure compare well with the volume-average values calculated using the EC_a values of the LBA-EUSTACH 1

Table 1
Comparison of aerosol refractive indices obtained from the iteration method with those derived from the volume-averaged chemical composition[a]

	Aerosol composition volume average (%)					Refractive index ($m = n - ik$)			
	POM	EC_a quartz (HVDS)	Hematite (Fe_2O_3)	INAM	Density (kg m^{-3})	n Composition quartz	k Composition quartz	n Iteration	k Iteration
(a) EC_a *content measured for quartz filter samples*									
LBA-EUSTACH 1 beginning (6–12 May 99)	52.1 ± 4.3	2.1 ± 0.2	0.3 ± 0.1	45.6 ± 4.0	1558 ± 25	1.45 ± 0.01	0.011 ± 0.001	1.42 ± 0.04	0.006 ± 0.003
LBA-EUSTACH 1 end (13–21 May 99)	64.7 ± 4.1	3.1 ± 0.3	0.4 ± 0.1	31.8 ± 3.5	1488 ± 27	1.44 ± 0.01	0.017 ± 0.004	1.46 ± 0.06	0.016 ± 0.003
LBA-EUSTACH 2 (12 Sep 31–Oct 99)	58.6 ± 4.0	1.4 ± 1.0	0	40.0 ± 3.8	1502 ± 24	1.44 ± 0.01	0.007 ± 0.001	1.41 ± 0.05	0.013 ± 0.005

	Aerosol composition volume average (%)				Refractive index ($m = n - ik$)			
	POM	BC_e Nuclepore (SFU)	INAM	Density (kg m^{-3})	n Composition Nuclepore	k Composition Nuclepore	n Iteration	k Iteration
(b) BC_e *content measured for Nuclepore filter samples*								
LBA-EUSTACH 1 beginning (6–12 May 99)	47.5 ± 4.1	10.6 ± 0.8	41.9 ± 3.3	1533 ± 21	1.46 ± 0.01	0.050 ± 0.004	1.42 ± 0.04	0.006 ± 0.003
LBA-EUSTACH 1 end (13–21 May .99)	60.6 ± 3.9	9.3 ± 0.9	30.1 ± 3.0	1472 ± 24	1.45 ± 0.01	0.044 ± 0.004	1.46 ± 0.06	0.016 ± 0.003
LBA-EUSTACH 2 (12 Sep–31 Oct 99)	57.3 ± 4.0	3.6 ± 0.3	39.1 ± 3.1	1496 ± 24	1.44 ± 0.01	0.017 ± 0.002	1.41 ± 0.05	0.013 ± 0.005

[a]Average values and standard deviation of the measurements are presented.

campaign; however, we could not reconcile the model results for LBA-EUSTACH 2 with the low average percentage values of EC_a measured for this campaign. The filter samples from LBA-EUSTACH 2 were heavily loaded, and, as noted above, the thermo-optical transmission technique may provide too low EC_a/OC ratios for such samples (Kubátová et al., 1999). Indeed, as LBA-EUSTACH 2 was characterized by intensive biomass burning, the percentage of EC_a in the fine aerosol sample is expected to be at least as high as during the other two periods. Alternatively, or additionally, the inability to reconcile the refractive index estimates could also be due to the fact that other absorbing materials besides EC_a are produced during the biomass burning process, including polyaromatic hydrocarbons (Finlayson-Pitts & Pitts, 2000) and polymeric organic compounds (Mukai & Ambe, 1986; Zappoli et al., 1999; Mayol-Bracero et al., 2002). However, as the OC quantity obtained by the TOT technique is by definition non-light absorbing, the refractive index value of $1.40 - 0i$ that we assume for POM does not take into account the presence of such light-absorbing organic compounds.

The imaginary refractive indices obtained using the BC_e values compare poorly with those calculated from the iteration model. We suspect that the high percentage of BC_e measured for LBA-EUSTACH 1 (about 10% of the volume) represents an overestimate of the true value. This could be attributed to the larger error associated with the determination of BC_e at low concentrations (i.e., LBA-EUSTACH 1). The LBA-EUSTACH 2 values of BC_e were obtained from measurements on highly loaded filters and there is better agreement between the refractive indices determined by the iteration and mass closure approaches.

3.3. Size distributions

We have compared the size distributions obtained from the PCASP instrument (after correction for the refractive index) to those measured with an MOUDI. The PCASP has an output of spherical-equivalent physical diameters, whereas the MOUDI (and all impactors in general) provides size distributions in terms of aerodynamic-equivalent diameters, D_a. D_a is the diameter of a sphere with a density equal to that of water (ρ_w) having the same terminal velocity as the particle impacted. In order to compare the two size distributions, the aerodynamic diameters were converted into geometric diameters, D. Assuming spherical particles of density ρ, the geometric diameter can be calculated from the aerodynamic diameter using the following equation (Willeke & Baron, 1993):

$$D = D_a \sqrt{\frac{\rho_w C_a}{\rho C}}, \tag{1}$$

where C and C_a are the Cunningham slip correction factors for D and D_a, respectively. We used the mass closure and densities established previously to determine an average aerosol density for each of the three periods defined above, and then applied these values to transform the size distribution measured by the MOUDI with the aid of Eq. (1). The calculated bulk densities of the fine aerosols obtained for the three periods are summarized in Table 1a. The same densities were assumed for the coarse mode particles. We also used the same average densities to calculate mass/size distributions from the number/size distributions of the PCASP. It should be cautioned that this approach does not take into account the presence of water or voids within the particles (Willeke & Baron, 1993). Therefore, the obtained geometric diameter falls into the definition of mass-equivalent diameter rather

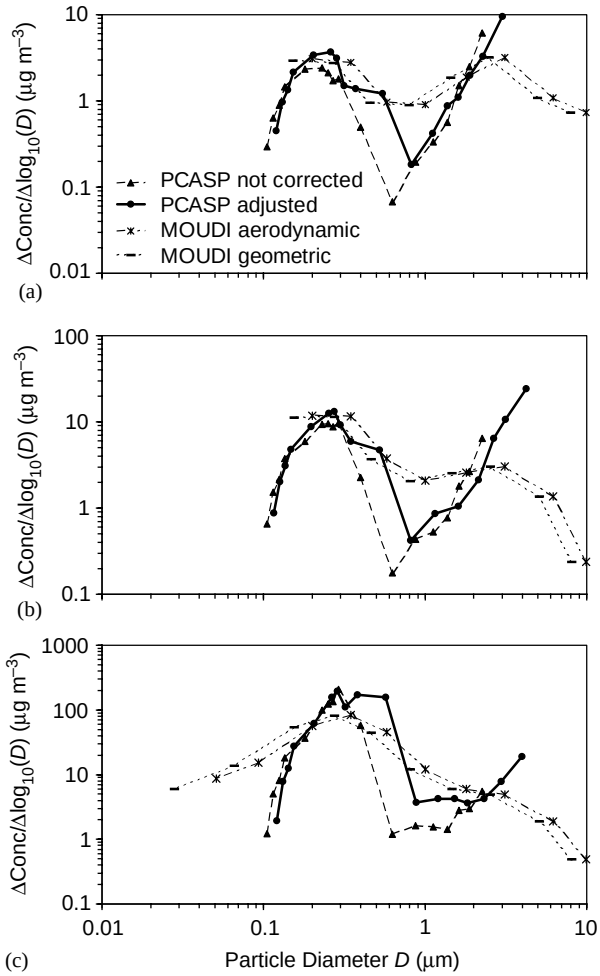

Fig. 5. Typical mass/size distributions obtained from the MOUDI and from the PCASP for the beginning (a) and the end (b) of the LBA-EUSTACH 1 campaign, and for the LBA-EUSTACH 2 campaign (c). The MOUDI samples were collected on 8–11 May 1999 (a), 17–20 May 1999 (b), and 5–6 October 1999 (c). The corrected and uncorrected size distributions are shown in each case.

than envelope-equivalent diameter. The "true" spherical-equivalent geometric diameter of the particles is probably somewhere in between the aerodynamic diameter and geometric diameter calculated as described above.

Figs. 5a–c show typical mass/size distributions obtained from the MOUDI and from the PCASP for the beginning and end of the LBA-EUSTACH 1 campaign, and for the LBA-EUSTACH 2 campaign. The original and the adjusted size distributions are shown in each case. For all three periods, bimodal distributions were found, with a fine mode centered at ca. 0.15–0.35 μm and a coarse mode at 2.3–4.2 μm. The fine-to-coarse mode ratio was found to increase from the beginning to the end of the LBA-EUSTACH 1 campaign, and then to the LBA-EUSTACH 2 campaign, due to the increasing contribution of biomass burning, which emits predominantly submicronic particles. It should be noted

that the last two stages of the MOUDI were not available during the first campaign, and that the size distributions presented are for particle sizes between 10 and 0.18 μm in eight stages only. Also, the smallest and the largest size bin of the PCASP are not presented, as the PCASP instrument does not have well-characterized upper and lower cutoff diameters; and the normalization over $\Delta \log_{10}(D)$ cannot be computed for these sizes. The observed shift in particle sizes (on the x-axis), between "PCASP not corrected" and "PCASP adjusted", and between "MOUDI aerodynamic" and "MOUDI geometric", is due to the correction of the particle size data of the PCASP (for the refractive index) and of the MOUDI (for the density), respectively. The shift in concentrations (on the y-axis) is due to the increase in the PCASP size bins from the adjustment in refractive index, and to the normalization over the difference of the logarithms of consecutive size bins.

It can be seen from Figs. 5a–c that adjusting the PCASP for the refractive index improves the agreement between the MOUDI and PCASP size distributions in the fine mode, but makes it worse for the coarse mode. The agreement in the fine aerosol mode between the two instruments is worse for the LBA-EUSTACH 2 data, with a large overestimation of the mass concentration from the PCASP. Note that assuming the commonly accepted specific density of 1000 kg m^{-3} for biomass burning aerosols (Radke et al., 1991), instead of the ca. 1500 kg m^{-3} we estimated, would lead to a more reasonable agreement.

In all three cases, coarse mode particle sizes obtained from the PCASP after adjustment for the refractive index are systematically larger than those obtained from the MOUDI. This effect is most likely due to the original assumption that the refractive index is the same over the whole size distribution. Such an assumption is the only option available with the PCASP size correction program distributed by the manufacturer, but it is also what is commonly assumed in modeling of aerosol optical properties or in retrieving aerosol properties from radiometer data. Although fine and coarse mode aerosol probably have a similar real refractive index component, it is very likely that the coarse mode has a lower imaginary part, because black carbon is usually concentrated in fine aerosols. Since the size bins of the adjusted PCASP size distribution increase as the imaginary refractive index component increases, this may explain the overestimation of the coarse mode particle sizes by the iteration procedure. This overestimation is less pronounced in Fig. 5a, probably partly because the calculated imaginary part of the refractive index was relatively low for the first period of the LBA-EUSTACH 1 campaign (Fig. 3a). Moreover, as discussed in Section 2.3.2, the coarse mode was estimated to have contributed 30–60% of the absorption for this period, demonstrating that the imaginary part of the refractive index for the coarse mode could have been about as high as for the fine mode during this part of the campaign. The assumption of a unique refractive index over the whole size distribution is, therefore, a reasonable one in this case. However, as the importance of absorption by aerosols in the fine mode increases due to increasing biomass-burning activity, the offset between the adjusted PCASP and MOUDI distributions becomes more noticeable (Figs. 5b and c).

Given that we may have systematically overestimated the size of the particles in the coarse mode by overestimating the amount of absorption by this mode, we decided to examine the effect of assuming the coarse mode to be completely non-absorbing. This is the other extreme to what we had assumed in our initial calculations (i.e., that the coarse mode is equally as absorbing as the fine), and it is likely that the "true" case lies somewhere between these two extremes. Table 2 presents a summary of these calculations, performed on one representative data set from each of the three periods described above.

Table 2
Influence of absorption by coarse mode aerosols on the total particle volume, and scattering (truncated) and absorption coefficients calculated using the iteration method. The measured values of (truncated) scattering and absorption coefficients are displayed in the first row of the table. The second row gives values obtained by Mie calculations applied to the uncorrected PCASP size distributions, using the refractive index of latex ($1.59 - 0i$). The third row shows the results obtained from the iteration procedure, and row four shows those obtained using the same real refractive index as in row three, but without taking the absorption component into account (k set to zero for the whole size distribution). The last row presents values obtained assuming the fine particle mode ($D < 1.35$ μm) to be the sole absorbing component of the aerosol

	LBA-EUSTACH 1 (7–12 May)			LBA-EUSTACH 1 (13–21 May)			LBA-EUSTACH 2		
Refractive index ($m = n - k$i)	Total volume ($\mu m^3\ cm^{-3}$)	Scattering coefficient (Mm^{-1})	Absorption coefficient (Mm^{-1})	Total volume ($\mu m^3\ cm^{-3}$)	Scattering coefficient (Mm^{-1})	Absorption coefficient (Mm^{-1})	Total volume ($\mu m^3\ cm^{-3}$)	Scattering coefficient (Mm^{-1})	Absorption coefficient (Mm^{-1})
Measured values	—	4.94	0.40	—	13.1	2.58	—	409	35.0
$1.59 - 0$i[a]	1.27	4.37	0.00	2.73	11.9	0.00	40.3	292	0.00
From iteration[a]	2.33	5.03	0.40	6.67	13.3	2.57	86.4	412	35.1
$k = 0$[a]	1.87	4.95	0.00	3.60	13.0	0.00	77.4	394	0.00
Coarse mode $k = 0$[b]	1.91	5.01	0.22	3.78	13.3	1.57	83.8	412	34.1

[a]A unique refractive index was applied over the whole size distribution.
[b]Real part of the refractive index applied over the whole size distribution. Coarse mode ($D > 1.35$ μm) assumed to be non-absorbing.

From Table 2 it is clear that using a refractive index of $1.59 - 0i$ leads to large differences between calculated and measured parameters, highlighting the need for the PCASP size distribution to be corrected for the refractive index before being used to calculate optical properties.

For LBA-EUSTACH 2, treating the coarse mode particles as non-absorbing has negligible effect on the calculated scattering coefficient, and leads to values of the absorption coefficient and total volume only 3% lower than the corresponding values obtained when all particles are assumed to be equally absorbing over the whole size distribution. This means that in the case of a very dominant, absorbing fine mode, considering the coarse mode to have the same refractive index as the fine mode leads to only small errors in the determination of the optical properties from the PCASP size distribution, and, conversely, little error in the determination of the refractive index, while reproducing the optical properties from the iteration. Neglecting absorption for both the fine and coarse mode leads to an underestimation of the scattering coefficient by only 4.4%; however, the total volume is ca. 7.6% lower than that calculated assuming the fine mode to be the only absorbing fraction.

Considering next the LBA-EUSTACH 1 campaign, the scattering coefficient can be reproduced equally for the beginning and end of the campaign, by treating the coarse mode as non-absorbing. The absorption coefficients for the two periods, however, are 45% and 39% lower than the values obtained when a constant refractive index is assumed, while the total volumes are 9% and 43% lower. This indicates that the coarse mode must have contributed substantially to the total absorption, in agreement with our other analyses (Section 2.3.2). For the beginning of the campaign, we have seen already that the corrected PCASP size distribution reproduces that measured by the MOUDI fairly well (Fig. 5a). This indicates that the use of a single refractive index to represent the whole size distribution is a reasonable approximation for this period, and moreover, that the real and imaginary part of the calculated effective refractive index are reasonable estimates for both the fine and the coarse modes. For the end of the campaign, however, the discrepancy between the adjusted PCASP and MOUDI distributions for the coarse mode is more noticeable, highlighting the inherent problems associated with obtaining accurate size distribution data from OPC instruments that use a single refractive index to represent the whole aerosol population.

3.4. Comparison with previous measurements

We now compare the refractive indices obtained from the iteration method to values found in the literature. It should be emphasized that the notion of refractive index becomes somewhat ill-defined when applied to inhomogeneous particles. Indeed, the refractive index of a complex mixture of compounds can only be expressed as an "equivalent refractive index" specific for the given measurement conditions and set of assumptions made about the properties of the aerosol. In our case, the calculated refractive indices can be defined as equivalent refractive indices for spherical, homogeneously internally mixed particles with the same bulk absorption and scattering properties as the actual particles. One should therefore remain cautious about drawing conclusions based on comparison of refractive indices of atmospheric aerosols obtained using different techniques. Table 3 shows a summary of refractive indices obtained using various techniques for biomass burning aerosols and for aerosols from remote conditions.

Our refractive index estimate for biomass burning aerosols is in the range of other values obtained recently, for the most part via sky radiance measurements (using a radiometer). However, the

Table 3
Refractive indices of biomass burning and background aerosols

Method	Wavelength (nm)	Relative humidity	Condition	Refractive index n; k	Reference
In situ size distribution, scattering, and absorption	545	Ambient, 48–80%	Biomass burning, Amazonian forest, Brazil (September–October 1999)	1.41 ± 0.05[a]; 0.013 ± 0.005[a]	This study
Sky radiance (AERONET radiometers)	440–1020[b]	Total column, not given	Biomass burning, Amazonian forest, Brazil (1993–1994) and Bolivia (1998–1999)	1.47 ± 0.03[a]; 0.0093 ± 0.003[a]	Dubovik et al., 2002
Sky radiance (AERONET radiometers)	440–1020[b]	Total column, not given	South American cerrado, Brazil	1.52 ± 0.01[a]; 0.015 ± 0.004[a]	Dubovik et al., 2002
Sky brightness (CIRATRA radiometers)	560–870[b]	"low" (ca. 50–80%) to "high" ($>80\%$)[c]	Southeast Asian forest fire haze (1997)	1.45 (1.37–1.55); k not given	von Hoyningen-Huene, Schmidt, Schienbein, Kee, & Tick, 1999
Sky radiance (AERONET radiometers)	440, 670, 870, and 1020	Total column, estimated "low"	Biomass burning, cerrado, Cuiabá, Brazil (1993–1994) and Bolivia (1998–1999)	1.53 ± 0.04[a,d], 1.55 ± 0.04[a,d], 1.59 ± 0.04[a,d], and 1.58 ± 0.04[a,d]; k not given	Yamasoe et al., 1998
Meteorology, aerosol, and radiative transfer model	500	Not given	Biomass burning, Canadian forest, July 1982	1.45–1.55; 0.01	Westphal and Toon, 1991
Remote sensing and in situ size (Langley LASE) distribution	815	"low" (30–50%) to "high" (80–100%)	Pollutant haze from United States over western Atlantic Ocean, July 1996 (TARFOX)	1.33–1.45; 0.001-0.008	Redemann et al., 2000
In Situ size distribution, scattering, and absorption	545	Ambient, 64–80%	Amazonian forest, background, Brazil (May 1999)	1.42 ± 0.04[a]; 0.006 ± 0.003[a]	This study
Transmittance	550	Not given	Rural	1.53; 0.006	Kent, Yue, Farrukh, & Deepak, 1983
Transmittance	550	Not given	Maritime/rural	1.474; 0.004	Kent et al., 1983
Various techniques	550	—	Dust like	1.53; 0.008	Kent et al., 1983; Dubovik et al., 2002 and references therein

[a]Standard deviation of the measurements.
[b]Refractive index of biomass burning aerosols spectrally independent over the range given.
[c]At ground level.
[d]Values dependent on wavelength.

Table 4

Parameter	LBA-EUSTACH 1 (7–12 May)	LBA-EUSTACH 1 (13–21 May)	LBA-EUSTACH 2 (20 September–25 October)	LBA-EUSTACH 2 (3 October)
(a) *Mie calculation (for a wavelength of 550 nm)*				
ω_0	0.93 ± 0.03	0.85 ± 0.02	0.90 ± 0.03	0.91 ± 0.02
g	0.63 ± 0.02	0.65 ± 0.03	0.70 ± 0.03	0.62 ± 0.02
β	0.12 ± 0.01	0.10 ± 0.01	0.08 ± 0.01	0.11 ± 0.01

	LBA-EUSTACH 1			LBA-EUSTACH 2		
Retrieved parameter	PCASP number concentration ± 5%	Scattering coefficient ± 5%	Absorption coefficient ± uncertainty	PCASP number concentration ± 10%	Scattering coefficient ± 5%	Absorption coefficient ± uncertainty
(b) *Maximum error obtained from the iteration method*						
ω_0	—	±1%	±2%	—	±2%	±2%
g	±6%	±5%	±1%	±8%	±4%	±1%
β	±11%	±11%	±2%	±20%	±10%	±1%

effective refractive index retrieved by this technique also requires the assumption that the aerosols are polydisperse, homogeneous, and spherical in shape.

Previous measurements of the refractive index of Amazonian background aerosols are, to our knowledge, non-existent. The lack of estimates from sky radiance measurements is due to the fact that this technique requires a relatively high aerosol loading (Dubovik et al., 2000). Therefore, we chose as a reference the well-accepted (Redemann et al., 2000) rural and maritime/rural values published by Kent et al. (1983) in a compilation of refractive indices. It is interesting to note that our estimate for the refractive index of Amazonian background aerosol is close to the value commonly accepted for dust particles ($m = 1.53 - 0.008i$), which was found to be a major component of the aerosols during the LBA-EUSTACH 1 campaign (see Section 2.3.2).

Generally, our estimates of the real refractive index component are lower than most previously reported values. As discussed in Section 3.2, this is mainly attributable to the high relative humidity conditions encountered during both field campaigns (see also Section 2.3.2). von Hoyningen-Huene et al. (1999) and Redemann et al. (2000) (Table 3) also obtained very low refractive index estimates under high RH conditions.

3.5. Single-scattering albedo, asymmetry parameter, and backscattered fraction

We also obtained other climatically relevant parameters from our iterative Mie calculations. Figs. 6a and b show the time series and Table 4a the averaged values of the single-scattering albedo (ω_0), asymmetry parameter (g), and backscattered fraction (β) (fraction of radiation scattered at scattering angles in the range of 90–180°) calculated at ambient RH $< 80\%$, for the LBA-EUSTACH 1 and 2 campaigns. The same sensitivity test was applied to these parameters as for the refractive index (Section 2.3.3). A summary of the maximum errors associated with variation of measured aerosol

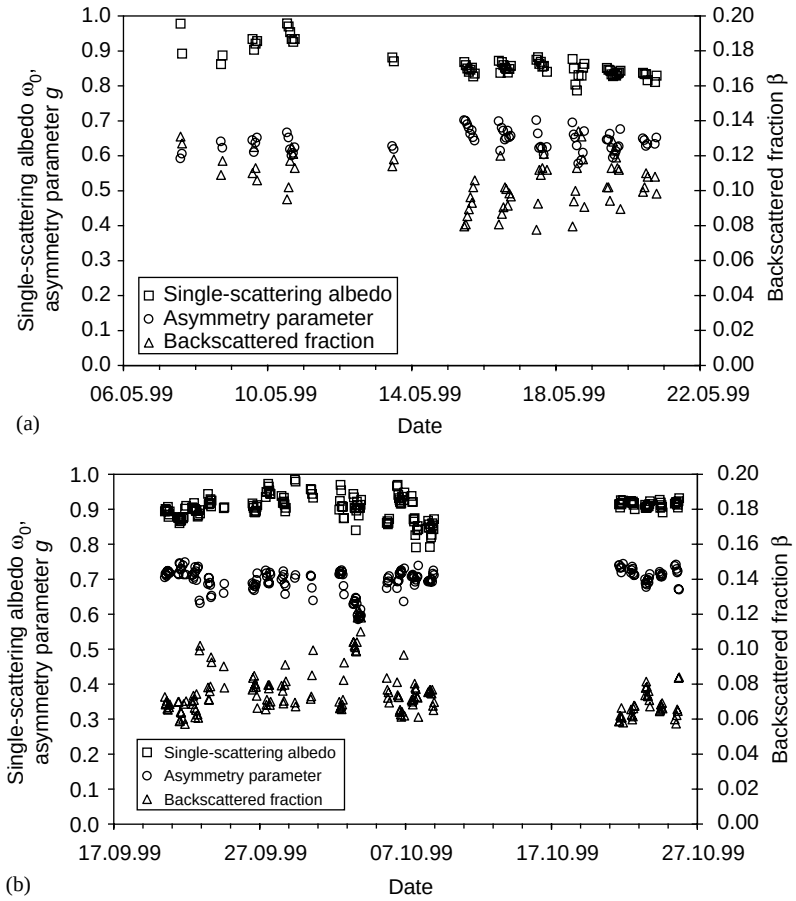

Fig. 6. (a) Single-scattering albedo, asymmetry parameter, and backscattered fraction calculated for the LBA-EUSTACH 1 campaign. The data were obtained from Mie calculations iterative procedure, using the PCASP size distribution, PSAP absorption, and nephelometer scattering data measured when ambient RH was $< 80\%$. (b) Single-scattering albedo, asymmetry parameter, and backscattered fraction calculated for the LBA-EUSTACH 2 campaign. The data were obtained from Mie calculations iterative procedure, using the PCASP size distribution, PSAP absorption, and nephelometer scattering data measured when ambient RH was $< 80\%$.

parameters is given Table 4b. The error associated with ω_0 and g was found to increase with decreasing values of ω_0 and g, whereas the error associated with β increased with increasing β.

The single-scattering albedo obtained from the Mie calculation differs from that calculated directly from the measured scattering and absorption coefficients, because the scattering coefficients were corrected for the truncation angle of the nephelometer. The relatively low average ω_0 value (0.85 ± 0.02) calculated for the end of the LBA-EUSTACH 1 campaign could be attributable to the aging process of the aerosols. Over the 2–3 days the aerosol particles traveled before being sampled (see Section 3.1), a black carbon core could have become enveloped in a non-absorbing shell due to cloud processing or uptake of gaseous species enhancing the absorption properties of the aerosols. Measurements under hazy conditions yielded average ω_0 values of 0.90 ± 0.03, which are higher

than, e.g., the values of 0.85 ± 0.02 (Cuiabá, Mato Grosso) and 0.86 ± 0.05 (Porto Velho, Rondônia) reported by Reid et al. (1998a) for SCAR-B (measurements performed at the same wavelength of 550 nm, with a comparable set of instrumentation). We note here that we would have obtained results similar to those presented by these authors, if we had not corrected the PSAP data according to Bond et al. (1999) ($\omega_0 = 0.86 \pm 0.04$).

The asymmetry parameter was found to increase, and the backscatter ratio to decrease, with increasing influence of fine particles, i.e., from the first part of LBA-EUSTACH 1 through to LBA-EUSTACH 2. Although this result may appear surprising since g usually increases (and β decreases) with increasing particle size for a given refractive index, it can be attributed to an increasing absorption efficiency of the aerosol (and imaginary refractive index component). This effect is particularly pronounced for very fine particles (smaller than 0.3 μm), as produced during biomass burning (Horvath, 1998). Our values of g for biomass burning haze compare well with those found by von Hoyningen-Huene et al. (1999) for Southeast Asian forest fire haze ($g = 0.69 \pm 0.02$). Dubovik et al. (2002) found g values of 0.69 ± 0.06 (at 440 nm) and 0.58 ± 0.06 (at 670 nm) for Amazonian forest biomass burning.

Reid et al. (1998a) reported β values of 0.11 to 0.12 ± 0.01 for Brazilian haze. These are larger than the average value we found for the biomass-burning season, but close to what we found on one particular day of the LBA-EUSTACH 2 campaign. The 3 October values were significantly different from the average background haze by virtue of a higher real refractive index part (with $m = 1.50\ (\pm 0.04) - 0.015\ (\pm 0.004)i$), a lower asymmetry parameter, and a higher backscatter fraction. Interestingly, the single-scattering albedo was close to the average. The larger n value implies a smaller correction to the PCASP size bins (for a constant value of k), and thus a greater relative contribution of smaller particles to the total population than found on average. Moreover, of all MOUDI samples collected in parallel to the online measurements, the sample collected on 3 October was the only one over the whole campaign for which stage number 8 (D_{50} equal to 0.200 μm) was the dominant fraction; all other samples typically showed a maximum loading on stage number 7 (D_{50} equal to 0.346 μm). These data all suggest that the aerosol measured on this particular day was likely young smoke aerosol derived from nearby burning.

4. Summary and conclusion

In this paper we have presented an original, robust method both for retrieving the effective refractive index of aerosols, and for correcting the measured size distribution derived from an OPC (PCASP), using data obtained from commercially available instruments in combination with standard Mie calculations. The method was applied to data sets obtained at an Amazonian tropical rainforest site during both background and biomass burning conditions. For periods when ambient RH was $< 80\%$, average refractive indices of $1.42 - 0.006i$ and $1.41 - 0.013i$ were estimated for background and biomass burning aerosols, respectively. The latter value compares well with literature values; however, there is only limited information available about the refractive index of background aerosols, particularly in the tropics. This is largely due to the fact that the commonly employed sky radiance method for retrieving refractive indices requires relatively high aerosol loadings. The application of our method may help to remedy this situation and facilitate the development of accurate radiation models.

A comparison of adjusted PCASP size distribution data with that obtained with an MOUDI indicates that reasonably accurate size distributions can be retrieved with an iterative method in cases when the fine mode dominates, or when the coarse mode has similar absorption properties to that of the fine. The use of a single effective refractive index to represent the aerosol population, however, prohibits reconciling these size distributions when the fine and coarse modes both contribute significantly to the total aerosol while having distinctly different optical properties. Our future work will focus on extending the current iteration method to allow for the use of two refractive indices to represent the two separate modes of the aerosol.

Acknowledgements

This work was carried out within the frame of the EUropean Studies on Trace gases and Atmospheric CHemistry (EUSTACH), a European contribution to the Large-Scale Biosphere-Atmosphere Experiment in Amazonia (LBA). It was financially supported by the Max Planck Society (MPG) and the Environmental and Climate Program of the European Union commission. One of us (W. M.) is indebted to the Belgian Federal Office of Scientific, Technical and Cultural Affairs (OSTC) for research support. The authors acknowledge MCT/INPE/CPTEC for providing the fire pixels data, Christof Ammann and Udo Rummel for providing the meteorological data, Xuguang Chi for assistance in the measurements with the thermal optical transmission instrument, and Carol Strametz for assistance editing the manuscript.

References

Anderson, T. L., Covert, D. S., Wheeler, J. D., Harris, J. M., Perry, K. D., Trost, B. E., Jaffe, D. J., & Ogren, J. A. (1999). Aerosol backscatter fraction and single-scattering albedo: Measured values and uncertainties at a coastal station in the Pacific northwest. *Journal of Geophysical Research-Atmospheres*, *104*, 26793.

Andreae, M. O. (1983). Soot carbon and excess fine potassium—long-range transport of combustion-derived aerosols. *Science*, *220*, 1148.

Andreae, M. O., Artaxo, P., Brandao, C., Carswell, F. E., Ciccioli, P., Costa, A. L. d., Culf, A. D., Esteves, J. L., Gash, J. H. C., Grace, J., Kabat, P., Lelieveld, J., Malhi, Y., Manzi, A. O., Meixner, F. X., Nobre, A. D., Nobre, C., Ruivo, M. d. L. P., Silva-Dias, M. A., Stefani, P., Valentini, R., Jouanne, J. v., & Waterloo, M. J. (2002). Towards an understanding of the biogeochemical cycling of carbon, water, energy, trace gases and aerosols in Amazonia: The LBA-EUSTACH experiment. *Journal of Geophysical Research-Atmospheres*, *107*, 8066. doi: 10.1029/2001JD000524.

Andreae, M. O., Artaxo, P., Fischer, H., Freitas, S. R., Gregoire, J. M., Hansel, A., Hoor, P., Kormann, R., Krejci, R., Lange, L., Lelieveld, J., Lindinger, W., Longo, K., Peters, W., de Reus, M., Scheeren, B., Dias, M., Ström, J., van Velthoven, P. F. J., & Williams, J. (2001). Transport of biomass burning smoke to the upper troposphere by deep convection in the equatorial region. *Geophysical Research Letters*, *28*, 951.

Artaxo, P., Martins, J. V., Yamasoe, M. A., Procópio, A. S., Pauliquevis, T. M., Andreae, M. O., Guyon, P., Gatti, L. V., & Leal, A. M. G. (2002). Physical and chemical properties of aerosols in the wet and dry season in Rondônia, Amazonia. *Journal of Geophysical Research-Atmospheres*, *107*, 8081. doi: 10.1029/2001JD000666.

Birch, M. E., & Cary, R. A. (1996). Elemental carbon-based method for monitoring occupational exposures to particulate diesel exhaust. *Aerosol Science and Technology*, *25*, 221.

Bond, T. C., Anderson, T. L., & Campbell, D. (1999). Calibration and intercomparison of filter-based measurements of visible light absorption by aerosols. *Aerosol Science and Technology*, *30*, 582.

Boucher, O., & Haywood, J. (2001). On summing the components of radiative forcing of climate change. *Climate Dynamics*, *18*, 297.

Collins, D. R., Jonsson, H. H., Seinfeld, J. H., Flagan, R. C., Gasso, S., Hegg, D. A., Russell, P. B., Schmid, B., Livingston, J. M., Ostrom, E., Noone, K. J., Russell, L. M., & Putaud, J. P. (2000). In situ aerosol-size distributions and clear-column radiative closure during ace-2. *Tellus Series B-Chemical and Physical Meteorology*, *52*, 498.

Dubovik, O., Holben, B., Eck, T. F., Smirnov, A., Kaufman, Y. J., King, M. D., Tanré, D., & Slutsker, I. (2002). Variability of absorption and optical properties of key aerosol types observed in worldwide locations. *Journal of the Atmospheric Sciences*, *59*, 590.

Dubovik, O., Smirnov, A., Holben, B. N., King, M. D., Kaufman, Y. J., Eck, T. F., & Slutsker, I. (2000). Accuracy assessments of aerosol optical properties retrieved from aerosol robotic network (AERONET) sun and sky radiance measurements. *Journal of Geophysical Research-Atmospheres*, *105*, 9791.

Ebert, M., Weinbruch, S., Rausch, A., Gorzawski, G., Helas, G., Hoffmann, P., & Wex, H. (2002). The complex refractive index of aerosols during LACE 98 as derived from the analysis of individual particles. *Journal of Geophysical Research-Atmospheres*, *107*, 8121. doi: 10.1029/2000JD000195.

Elbert, W., Hoffmann, M. R., Kramer, M., Schmitt, G., & Andreae, M. O. (2000). Control of solute concentrations in cloud and fog water by liquid water content. *Atmospheric Environment*, *34*, 1109.

Finlayson-Pitts, B. J., & Pitts, J. N. (2000). *Chemistry of the upper and lower atmosphere theory, experiments and applications*. San Diego: Academic Press.

Fuller, K. A., Malm, W. C., & Kreidenweis, S. M. (1999). Effects of mixing on extinction by carbonaceous particles. *Journal of Geophysical Research-Atmospheres*, *104*, 15941.

Guyon, P., Graham, B., Roberts, G. C., Mayol-Bracero, O. L., Maenhaut, W., Artaxo, P., & Andreae, M. O. (2003). In-canopy gradients, composition, sources, and optical properties of aerosol over the Amazon forest. *Journal of Geophysical Research-Atmospheres*, accepted for publication.

Hallett, J., Hudson, J. G., & Rogers, C. F. (1989). Characterization of combustion aerosols for haze and cloud formation. *Aerosol Science and Technology*, *10*, 70.

Hoppel, W. A., Fitzgerald, J. W., Frick, G. M., Larson, R. E., & Mack, E. J. (1990). Aerosol size distributions and optical-properties found in the marine boundary-layer over the Atlantic-Ocean. *Journal of Geophysical Research-Atmospheres*, *95*, 3659.

Horvath, H. (1998). Influence of atmospheric aerosols upon the global radiation balance. In: R. M. Harrison, R. Van Grieken (Eds.), *Atmospheric particles*. New York: Wiley. p. 543.

Kent, G. S., Yue, G. K., Farrukh, U. O., & Deepak, A. (1983). Modeling atmospheric aerosol backscatter at CO_2-laser wavelengths. 1. Aerosol properties, modeling techniques, and associated problems. *Applied Optics*, *22*, 1655.

Kubátová, A., Vermeylen, R., Claeys, M., Cafmeyer, J., & Maenhaut, W. (1999). Carbonaceous aerosols and particulate organic compounds in Gent, Belgium, during winter and summer of 1998. *Journal of Aerosol Science*, *30*(Suppl. 1), S905.

Liu, Y. G., & Daum, P. H. (2000). The effect of refractive index on size distributions and light scattering coefficients derived from optical particle counters. *Journal of Aerosol Science*, *31*, 945.

Marley, N. A., Gaffney, J. S., Baird, C., Blazer, C. A., Drayton, P. J., & Frederick, J. E. (2001). An empirical method for the determination of the complex refractive index of size-fractionated atmospheric aerosols for radiative transfer calculations. *Aerosol Science and Technology*, *34*, 535.

Martins, J. V., Hobbs, P. V., Weiss, R. E., & Artaxo, P. (1998). Sphericity and morphology of smoke particles from biomass burning in Brazil. *Journal of Geophysical Research-Atmospheres*, *103*, 32051.

Mason, B., & Moore, C. B. (1982). *Principles of geochemistry*. New York: Wiley.

Mayol-Bracero, O. L., Guyon, P., Graham, B., Roberts, G., Andreae, M. O., Decesari, S., Facchini, M. C., Fuzzi, S., & Artaxo, P. (2002). Water-soluble organic compounds in biomass burning aerosols over Amazonia: 2. Apportionment of the chemical composition and importance of the polyacidic fraction. *Journal of Geophysical Research-Atmospheres*, *107*, 8091. doi: 10.1029/2001JD000522.

Miller, J. M., Whelpdale, D. M., Barrie, L. A., Isaksen, I. S. A., Rodhe, H., & Smith, F. B. (1985). The transport of sulfur and nitrogen through the remote atmosphere. In J. N. Galloway, R. J. Charlson, M. O. Andreae, H. Rodhe, D. Reidel (Eds.), *The biogeochemical cycling of sulfur and nitrogen in the remote atmosphere*. (p. 127). Mass: Hingham.

Mishchenko, M. I., Travis, L. D., Kahn, R. A., & West, R. A. (1997). Modeling phase functions for dustlike tropospheric aerosols using a shape mixture of randomly oriented polydisperse spheroids. *Journal of Geophysical Research-Atmospheres*, *102*, 16831.

Mukai, H., & Ambe, Y. (1986). Characterization of a humic acid-like brown substance in airborne particulate matter and tentative identification of its origin. *Atmospheric Environment*, *20*, 813.

Pesava, P., Horvath, H., & Kasahara, M. (2001). A local optical closure experiment in vienna. *Journal of Aerosol Science*, *32*, 1249.

Pickering, K. E., Thompson, A. M., Wang, Y. S., Tao, W. K., McNamara, D. P., Kirchhoff, V., Heikes, B. G., Sachse, G. W., Bradshaw, J. D., Gregory, G. L., & Blake, D. R. (1996). Convective transport of biomass burning emissions over Brazil during TRACE A. *Journal of Geophysical Research-Atmospheres*, *101*, 23993.

Radke, L. F., Hegg, D. A., Hobbs, P. V., Nance, J. D., Lyons, J. H., Laursen, K. K., Weiss, R. E., Riggan, P. J., & Ward, D. E. (1991). Particulates and trace gas emissions from large biomass fires in North America. In J. S. Levine (Eds.), *Global biomass burning*: *Atmospheric*, *climatic*, *and biospheric implications*. (p. 209). Cambridge: MIT Press.

Redemann, J., Turco, R. P., Liou, K. N., Russell, P. B., Bergstrom, R. W., Schmid, B., Livingston, J. M., Hobbs, P. V., Hartley, W. S., Ismail, S., Ferrare, R. A., & Browell, E. V. (2000). Retrieving the vertical structure of the effective aerosol complex index of refraction from a combination of aerosol *in situ* and remote sensing measurements during TARFOX. *Journal of Geophysical Research-Atmospheres*, *105*, 9949.

Reid, J. S. (1998). *Emission, evolution, and radiative properties of particles from biomass burning in Brazil*. Ph.D. thesis, University of Washington, Washington.

Reid, J. S., Hobbs, P. V., Ferek, R. J., Blake, D. R., Martins, J. V., Dunlap, M. R., & Liousse, C. (1998a). Physical, chemical, and optical properties of regional hazes dominated by smoke in Brazil. *Journal of Geophysical Research-Atmospheres*, *103*, 32059.

Reid, J. S., Hobbs, P. V., Liousse, C., Martins, J. V., Weiss, R. E., & Eck, T. F. (1998b). Comparisons of techniques for measuring shortwave absorption and black carbon content of aerosols from biomass burning in Brazil. *Journal of Geophysical Research-Atmospheres*, *103*, 32031.

Savoie, D. L., Prospero, J. M., & Nees, R. T. (1987). Nitrate, non-sea-salt sulfate, and mineral aerosol over the northwestern Indian-Ocean. *Journal of Geophysical Research-Atmospheres*, *92*, 933.

Sokolik, I. N., & Toon, O. B. (1999). Incorporation of mineralogical composition into models of the radiative properties of mineral aerosol from UV to IR wavelengths. *Journal of Geophysical Research-Atmospheres*, *104*, 9423.

Solomon, P. A., Moyers, J. L., & Fletcher, R. A. (1983). High-volume dichotomous virtual impactor for the fractionation and collection of particles according to aerodynamic size. *Aerosol Science and Technology*, *2*, 455.

Staudt, A. C., Jacob, D. J., Logan, J. A., Bachiochi, D., Krishnamurti, T. N., & Sachse, G. W. (2001). Continental sources, transoceanic transport, and interhemispheric exchange of carbon monoxide over the Pacific. *Journal of Geophysical Research-Atmospheres*, *106*, 32571.

Stolzenburg, M., Kreisberg, N., & Hering, S. (1998). Atmospheric size distributions measured by differential mobility optical particle size spectrometry. *Aerosol Science and Technology*, *29*, 402.

Turpin, B. J., & Lim, H. J. (2001). Species contributions to PM2.5 mass concentrations: Revisiting common assumptions for estimating organic mass. *Aerosol Science and Technology*, *35*, 602.

von Hoyningen-Huene, W., Schmidt, T., Schienbein, S., Kee, C. A., & Tick, L. J. (1999). Climate-relevant aerosol parameters of South-East-Asian forest fire haze. *Atmospheric Environment*, *33*, 3183.

Westphal, D. L., & Toon, O. B. (1991). Simulations of microphysical, radiative, and dynamic processes in a continental-scale forest-fire smoke plume. *Journal of Geophysical Research-Atmospheres*, *96*, 22379.

Willeke, K., & Baron, P. A. (1993). *Aerosol measurements: Principles, techniques, and applications*. New York: Van Nostrand Reinhold.

Yamasoe, M. A., Kaufman, Y. J., Dubovik, O., Remer, L. A., Holben, B. N., & Artaxo, P. (1998). Retrieval of the real part of the refractive index of smoke particles from sun/sky measurements during SCAR-B. *Journal of Geophysical Research-Atmospheres*, *103*, 31893.

Yu, J. Z., Xu, J. H., & Yang, H. (2002). Charring characteristics of atmospheric organic particulate matter in thermal analysis. *Environmental Science and Technology*, *36*, 754.

Zappoli, S., Andracchio, A., Fuzzi, S., Facchini, M. C., Gelencser, A., Kiss, G., Krivacsy, Z., Molnar, A., Meszaros, E., Hansson, H. C., Rosman, K., & Zebuhr, Y. (1999). Inorganic, organic and macromolecular components of fine aerosol in different areas of Europe in relation to their water solubility. *Atmospheric Environment*, *33*, 2733.